DOI: 10.1002/chem.200700216

The Stuffed Framework Structure of SrP_2N_4: Challenges to Synthesis and Crystal Structure Determination

Friedrich W. Karau,[a] Lena Seyfarth,[b] Oliver Oeckler,[a] Jürgen Senker,[b] Kai Landskron,[a, c] and Wolfgang Schnick*[a]

Abstract: SrP_2N_4 was obtained by high-pressure high-temperature synthesis utilizing the multianvil technique (5 GPa, 1400 °C) starting from mixtures of phosphorus(V) nitride and strontium azide. SrP_2N_4 turned out to be isotypic with $BaGa_2O_4$ and is closely related to $KGeAlO_4$. The crystal structure (SrP_2N_4, $a = 17.1029(8)$, $c = 8.10318(5)$ Å, space group $P6_3$ (no. 173), $V = 2052.70(2)$ Å^3, $Z = 24$, $R(F^2) = 0.0633$) was solved from synchrotron powder diffraction data by applying a combination of direct methods, Patterson syntheses, and difference Fourier maps adding the unit cell information derived from electron diffraction and symmetry information obtained from ^{31}P solid-state NMR spectroscopy. The structure of SrP_2N_4 was refined by the Rietveld method by utilizing both neutron and synchrotron X-ray powder diffraction data, and has been corroborated additionally by ^{31}P solid-state NMR spectroscopy by employing through-bond connectivities and distance relations.

Keywords: electron diffraction · electron microscopy · high-pressure chemistry · neutron diffraction · solid-state NMR spectroscopy · X-ray diffraction

Introduction

A number of nitrides have been found that exhibit structural analogies with oxides. Both the wurtzite (e.g. AlN) and antibixbyite structure-type (e.g. alkaline-earth metal nitrides) have been found frequently and even a nitridic perovskite $ThTaN_3$ has been reported.[1] Tetrahedral networks with a composition AX_2 are of special interest because they might exhibit structural analogies with SiO_2 or alumosilicates. A series of nitridophosphate network structures $[PN_2]^-$ are known[2–4] that are formally isoelectronic with SiO_2. However, structural similarities with known oxosilicates have scarcely been identified: Phosphorus nitride imide $PN(NH)$[5,6] at ambient pressure adopts a structure homeotypic with the *cristobalite* structure type and both $LiPN_2$[7,8] and $NaPN_2$[9,10] crystallize analogously adopting the *chalcopyrite* structure type. Furthermore, a series of *nitridosodalites*[11–15] and *oxonitridosodalites*[16] have been found. In contrast, alkaline-earth nitridophosphates of the composition MP_2N_4 exhibit more similarities with oxo- and thiogallates,[17,18] oxogermanates,[19] and high-pressure oxoborates,[20] respectively (e.g. BaP_2N_4,[2] $BaSr_2P_6N_{12}$,[3] and $BaCa_2P_6N_{12}$[3] whose structures are derived from a high-pressure phase of CaB_2O_4[20] and $BaGa_2S_4$,[18] respectively).

Herein we report on SrP_2N_4 whose structure solution has been hampered by the unavailability of single crystals and the presence of a complex superstructure. Finally, the structure solution was possible by employing a combination of different diffraction methods (synchrotron X-ray, neutron, and electron diffraction), electron microscopy as well as solid-state NMR spectroscopy. A similar complementary combination of investigation methods has recently served as the ultimate structure solution tool.[21,22] This approach enabled us to solve the crystal structure with a significantly higher accuracy than typical for powder data. Beyond this it opens up the rare possibility to judge the expressiveness of the individual techniques for a complicated example of an

[a] Dr. F. W. Karau, Dr. O. Oeckler, Prof. Dr. K. Landskron, Prof. Dr. W. Schnick
Department Chemie und Biochemie
Ludwig-Maximilians-Universität München
Butenandtstrasse 5–13 (D), 81377 München (Germany)
Fax: (+49) 89-2180-77440
E-mail: wolfgang.schnick@uni-muenchen.de

[b] L. Seyfarth, Prof. Dr. J. Senker
Anorganische Chemie I der Universität Bayreuth
Universitätsstrasse 30, 95447 Bayreuth (Germany)

[c] Prof. Dr. K. Landskron
New address:
Department of Chemistry, Lehigh University
6 East Packer Avenue, Bethlehem, PA 18015 (USA)

ab initio structure solution based on powder diffraction data.

Results and Discussion

Challenges to the synthesis: High N_2 partial pressures, which are available by in situ thermolysis of azides, have been used frequently[2–4] for the synthesis of metal-containing nitridophosphates starting from the respective metal azides and P_3N_5. Thereby, phosphorus nitride P_3N_5,[23] which already decomposes above 850 °C at ambient pressure, is prevented from dissociation into the elements [Eq. (1)] at the high reaction and recrystallization temperatures above 1000 °C.

$$P_3N_5 \rightleftharpoons 3\,PN + N_2 \rightleftharpoons 3/4\,P_4 + 5/2\,N_2 \quad (1)$$

Increasing the N_2 partial pressure (5–15 GPa) promotes the reverse reaction of Equation (1), following the law of mass action. The metal azide supplies the necessary nitrogen (see Equation (2)) and transforms to the respective metal nitride intermediately, which reacts in situ with P_3N_5 forming the desired nitridophosphate.[2]

$$3\,M^{+II}(N_3)_2 + 2\,P_3N_5 \rightarrow \text{“}M^{+II}{}_3N_2\text{”} + 8\,N_2 + 2\,P_3N_5 \rightarrow 3\,M^{+II}\,P_2N_4 + 8\,N_2$$
$$M^{+II} = Cd, Be \ldots Ba \quad (2)$$

To achieve these reaction conditions, we employed the multianvil technique,[24,25] which makes available both high N_2 partial pressures and temperatures above 1000 °C (see Experimental Section).

Challenges to the crystal structure analysis: Highly condensed phosphorus nitrides suffer from crystallizing poorly, because they cannot be heated without thermolysis close to their extrapolated melting point, even at high N_2 partial pressures. Transmission electron microscopic (TEM) investigations exhibit crystallites of SrP_2N_4 in the range 200–800 nm. Therefore, the crystallographic characterization of SrP_2N_4 has been performed by powder methods. SrP_2N_4 was first synthesized and characterized by Landskron et al.,[26] however, the structure refinement was not satisfactorily due to a lack of crystallinity and quality of the diffraction data. Additionally, SrP_2N_4 forms a superstructure leading to a complex powder pattern, which is not indexable even if synchrotron radiation is used (see Figure 1 and Experimental Section). Simply the basic unit cell (hexagonal cell obtained from a LeBail refinement: $a=9.8769(3)$, $c=8.1050(3)$ Å, $V=684.74(4)$ Å^3) could be obtained with the Werner[27] or Visser[28] algorithm using the strongest reflections solely.[1] The weak hexagonal superstructure cell ($a=17.10$, $c=8.10$ Å, $V=2050$ Å^3) was indexed from electron diffraction tilting series and refined by a LeBail fit ($a=17.1029(8)$, $c=8.10318(5)$ Å, $V=2052.70(2)$ Å^3). Tilting series about a^* and b^* prove the symmetry not to be trigonal, because pairs of diffraction images with the same tilt about a^* and b^* exhibit the same pattern. After determination of the unit cell, possible space groups were determined.

[1] For example, the intensity of the 422 superstructure reflection (one of the strongest) is only 0.52 % of the 222 reflection already appearing in the diffractogram for the basic structure.

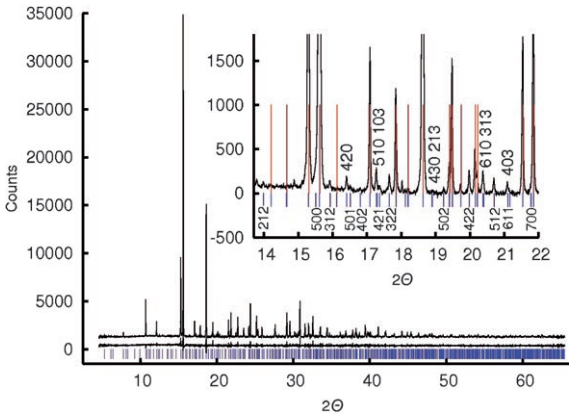

Figure 1. Synchrotron powder diffraction pattern and Rietveld refinement of SrP_2N_4 with measured histogram, difference curve, and allowed reflection positions (bars). The inset shows a cut-out of the histogram. The main reflections appearing for the basic structure as well are marked with long, dashed, red bars; the reflections of the superstructure are marked with short blue bars.

Valuable information about the space group can be provided by solid-state NMR as the number and intensity of resonances directly correspond to the number and multiplicity of crystallographically inequivalent sites (see also reference [29]). We thus measured a fully relaxed ^{31}P MAS spectrum at a field B_0 of 17.62 T ($\nu_0=303.7$ MHz, Figure 2a). At first glance the spectrum exhibits five signals (A–E) with an intensity ratio 1:1:3:2:1 (Figure 2a). Furthermore, by employing a ^{31}P RIL experiment the phase homogeneity was demonstrated (Figure 2c). A RIL sequence probes spatial proximities and the chosen mixing time of 20 ms corresponds to a spin-diffusion radius of about 30 Å. The line-

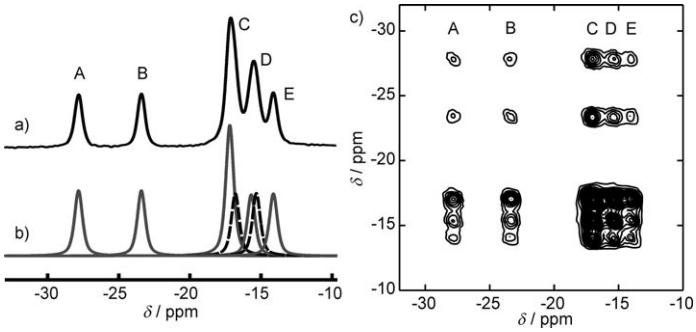

Figure 2. a) 1D MAS NMR spectrum of SrP_2N_4 recorded at $\nu_0=303.7$ MHz. Letters A to E will be used in the text to refer to the five signals; b) deconvolution of (a) with equal widths for all resonances results in seven signals with intensities 1:1:2:1:1:1:1; c) 2D MAS NMR RIL spectrum of SrP_2N_4 ($\nu_0=202.5$ MHz) with a mixing time of 20 ms. Off-diagonal peaks arise only for spatially neighboured nuclei ($d<30$ Å).

widths for the signals C and D in the 1D spectrum (Figure 2a) are considerably broader (FWHH $\approx$250 Hz) than the ones for the resonances A, B, and E (FWHH $\approx$200 Hz). The broadening of the signals C and D may be caused by three different mechanisms, which should be discussed briefly in the following. First, the ^{31}P signal may be broadened due to a second-order coupling to the neighboring quadrupolar nuclei ^{14}N. This mechanism is proportional to the strength of the external magnetic field and should become more pronounced at lower fields. Measurements at $\nu_0 =$ 162.0 MHz (9.4 T) and 202.5 MHz (11.7 T), however, reveal similar or even smaller linewidths rendering an influence of this effect on the observed ^{31}P linewidths highly improbable. Second, anisotropic size distributions of small crystals may lead to distributions of the chemical shift parameters and thus cause varying linewidths in the MAS spectrum. However, the diagonal peaks of the RIL spectrum (Figure 2c) are nearly as broadened as the cross peaks, which demonstrates that the crystallites are significantly larger than the spin-diffusion range in the RIL experiment. Thus it is unlikely that the broadening of the signals C and D is caused by this effect either.

Most probably, the linewidths of the signals C and D originate from crystallographically inequivalent ^{31}P nuclei with similar but not identical isotropic chemical shifts. Since the resolution of a 1D spectrum increases with increasing B_0, a splitting of such resonances becomes more pronounced at higher fields and thus leads to a broadening effect. Only the more intensive signals C and D broaden at higher external field, which is in perfect agreement with the latter hypothesis.

Consequently, we deconvoluted the 1D spectrum by assuming multiple resonances with however equal line widths for the signal groups C and D (Figure 2b). This reveals seven resonances with intensities A:B:C1:C2:D1:D2:E = 1:1:2:1:1:1:1. Assuming the resonance with the highest intensity (C1) to represent P atoms on the general crystallographic position (multiplicity $y = n$) all other resonances have to belong to P atoms on special positions with a multiplicity of $n/2$. However, for hexagonal space groups special positions underlie strong restrictions, which are unlikely to be met for dense networks as in SrP_2N_4. Thus it seems to be much more reasonable that the structure of SrP_2N_4 exhibits eight resonances with equal intensities corresponding to eight crystallographically independent P atoms on general positions. All further NMR experiments were performed at lower fields where the resonances of the signals C and D are not resolved (for labeling of signals see Figure 2a).

Microfocus electron beam diffraction images in [001] (Figure 3) exhibit the Laue class 6/*m* and *no* twofold rotation axes orthogonal to the crystallographic *c* axis. From the comparison of the microfocus diffraction pattern in [001] and the SAED diffraction pattern in the same direction with full beam (Figure 3) it could be concluded that the SrP_2N_4 crystallites are obviously twins in most of the cases, as the SAED diffraction patterns *exhibit* twofold axes in the a^*b^* plane. Typically, the framework density[31] of nitridophosphates with SiO_2 isoelectronic framework ranges between 22–25 T/1000 Å^3.[2–4] With eight P sites of equal multiplicity, we estimated P atoms to occupy a site with multiplicity six. From the hexagonal space groups with Laue symmetry 6/*m* we considered those with the group symmetry *p*6 along [001] and *pg* along [010] ($b' = c$), as determined from HRTEM images (Figures 4, 5, and 6). On the basis of these restrictions, only the space groups $P6_1$ (no. 169), $P6_5$ (no. 170), and $P6_3$ (no. 173) had to be taken into account for the structure solution.

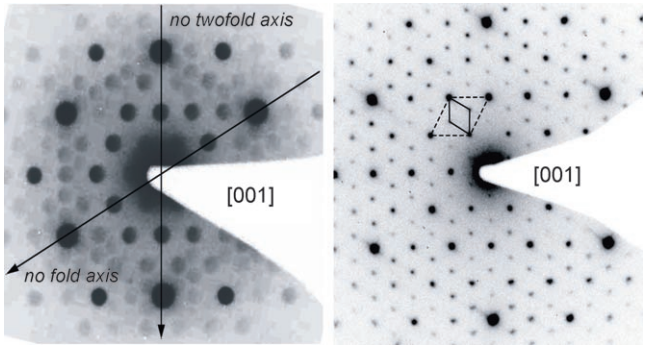

Figure 3. Microfocus electron diffraction pattern (zone axis [001]) (left image). Apparently, there are no twofold axes along the arrows (a^* b^* plane). The reflections left and right to the axis do not have the same intensity. Full beam electron diffraction pattern (zone axis [001], right image). Apparently there are twofold axes in the a^* b^* plane. This is due to twinning. The reciprocal unit cell of the basic structure cell is drawn in dashed lines, the reciprocal superstructure cell in solid lines.

A "model biased" LeBail intensity and F_o^2 extraction[2] and unit cell refinement was performed on the basis of the synchrotron powder diffraction data for the three possible space groups using the program package GSAS.[32] The pro-

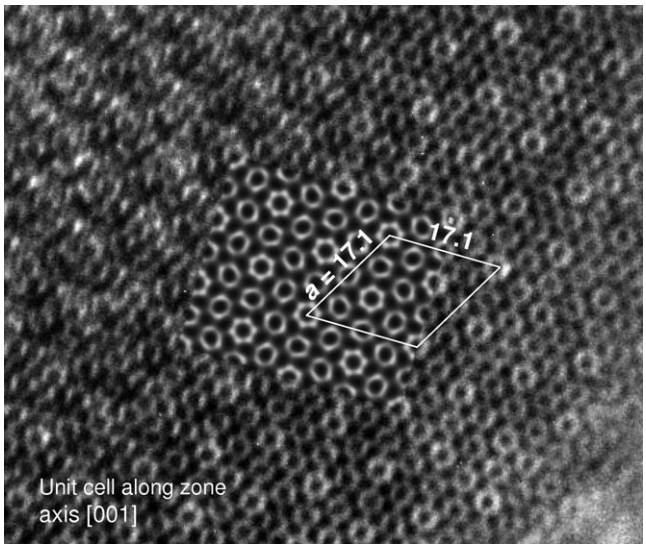

Figure 4. HRTEM image perpendicular to [001] and simulation. The elementary mesh is drawn with white lines (units in Å).

[2] The F_o^2 extraction was biased by placing a Sr atom on 000.

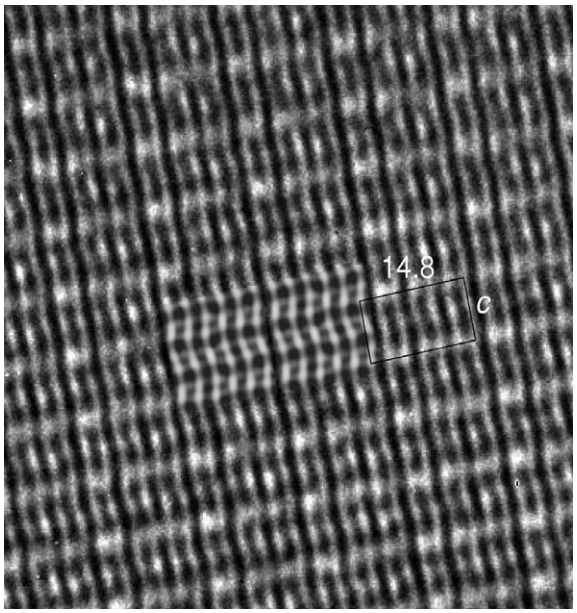

Figure 5. HRTEM image perpendicular to [010] and simulation. The elementary mesh is drawn with black lines (units in Å).

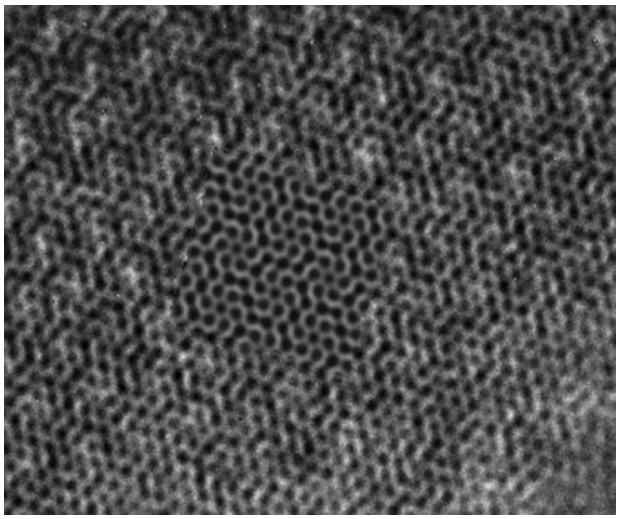

Figure 6. HRTEM image perpendicular to [001] and simulation.

cedure is—except for the model biasing—similar to the one described in the literature.[33,34] Initially, the heavy atoms (Sr) were located by direct methods (SHELXS[35]), subsequently the P atoms and only a few N atoms could be added consecutively by direct methods (SHELXS[35]) and evaluation of Patterson maps (GSAS[32]). After each of these steps a Rietveld refinement of the fragmentary structure model was undertaken (GSAS[32]) to obtain more reliable F_o^2 values. The remaining N atoms were added by evaluating a difference Fourier map calculated with the program package GSAS.[32] A successful structure solution could be performed only in space group $P6_3$ with lattice constants $a=17.1029(8)$, $c=8.10318(5)$ Å, $V=2052.70(2)$ Å^3, $Z=24$. Finally, a Rietveld refinement with the complete structure model was performed (GSAS, $R(F^2)=0.0633$, $wRp=0.0926$, $Rp=0.0737$, Figure 1, Table 1). The isotropic thermal displacement parameters for the N atoms, the P atoms, and the Sr atoms, respectively, were refined and set to be equal in each case. To obtain more accurate thermal displacement parameters and to verify the crystal structure by utilizing a different contrast for the atomic scattering factors (especially the N atom positions), a Rietveld refinement based on neutron powder diffraction data (D20 diffractometer, ILL Grenoble, France, Table 1) was performed (Figure 7). The thermal displacement parameters of the most intensely scattering atoms (i.e. N and Sr) could be refined individually, whereas those of the P atoms were set to be equal (Table 2). Instead of the lattice parameters the error-prone wavelength of the neutron data was refined against the more accurate lattice parameters taken from the synchrotron data refinement. The atomic parameters, within the accuracy (3σ) of both synchrotron and neutron diffraction, turned out to be identical.

Table 1. Crystallographic data for SrP_2N_4 (synchrotron and neutron radiation).[a]

	Synchrotron radiation	Neutron radiation
radiation [Å]	0.7996003 (sync.)	1.8893(1) (refined)
formula	SrP_2N_4	
crystal system, lattice parameters	hexagonal, $P6_3$ (no. 173)	
a [Å]	17.1029(8)	17.1029
c [Å]	8.10317(5) (refined)	8.10317 (not ref.)
a/c	2.1106	
formula units	24	
cell volume [Å^3]	2052.69(2)	2052.69(6)
formula mass [g mol^{-1}]	205.596	
X-ray dens. [g cm^{-3}]	3.992	
diffractometer	SNBL-beamline, Grenoble	D20 Diffractometer, ILL Grenoble, France
detector	Tl/NaI	1600 cell (PSD), $^3He/CF_4$
absorption correction	Lobanov & Alte da Veiga for Debye Scherrer geometry[66]	none
internal step [°] width	0.005	0.025
$N_{obs.}$	1930	853
data points	12185	5865
step width [°]	0.005	0.0235
2θ range [°]	4.552–65.477	7.16–144.99
background function coefficients	shifted Chebyshev 14	6
profile function	pseudo Voigt	
R values		
wRp	0.0928	0.0638
Rp	0.0737	0.0483
wRp_{Bknd}	0.0926	0.0802
Rp_{Bknd}	0.0742	0.0604
$R(F^2)$	0.0633	0.0873

[a] Further details of the crystal structure analysis may be obtained from the Fachinformationszentrum Karlsruhe, D-76344 Eggenstein-Leopoldshafen (Germany), by quoting the depository number CSD-416930 (SrP_2N_4).

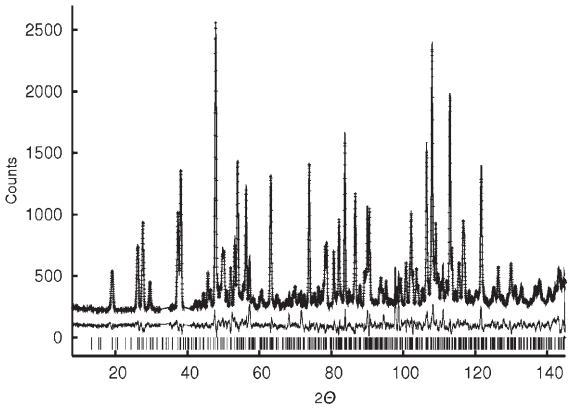

Figure 7. Neutron powder diffraction pattern and Rietveld refinement of SrP_2N_4. Measured histogram (line), calculated pattern (crosses), difference curve and allowed reflections (bars).

The crystallographic data of both measurements are given in Table 1, and the atomic positions and thermal displacement parameters are given in Table 2. Based on this structure model, multislice simulations (program package EMS[36]) of *h*igh *r*esolution *t*ransmission *e*lectron *m*icrographs (HRTEM) along [001] and [010] were compared with the images of some microcrystals along the same crystallographic direction (Figures 4–6). The simulations fit well into the acquired images and confirm the refined structure model. Especially in images for the zone axis [001], the unit cell dimensions are obvious as well as the 6_3 axes, which appear as sixfold axes in the HRTEM image (Figure 4).[3] They penetrate the image plane at the corners of the elementary mesh. The six-ring pattern about the 6_3 axis, can be clearly distinguished from the distorted six-rings lying between the regular ones and having twofold axes in the HRTEM image (Figure 4); they are about the 2_1 axis (see Figure 12 respectively).

To confirm the results from the diffraction data with an independent method a detailed solid-state NMR analysis of SrP_2N_4 with various 2D MAS experiments was performed. In the literature some examples are reported[37–40] where such a combination of experiments could successfully validate structures from powder diffraction analysis. To the best of our knowledge, however, none of these examples deals with such a heavy spectral overlap (Figure 2a) of NMR resonances as it is given in SrP_2N_4. In reference [37] it is pointed out that such a poor spectral resolution will pose an additional challenge to the structure confirmation with solid-state NMR spectroscopy. For our analysis we adapted an approach proposed by Helluy et al.[40] for phosphates. The NMR interactions employed there are the direct and the indirect (J) dipolar couplings. While the J coupling probes through-bond connectivities and thus can help to assign the eight crystallographical P sites to the five NMR signals, the direct dipolar coupling is sensitive to distances. Unfortunately, for abundant spins like ^{31}P in a highly condensed network

[3] One can conclude only the Patterson symmetry from HRTEM images.

Table 2. Wyckoff position, atomic positions and isotropic thermal displacement parameters (in 0.01 Å^2) (first row for each atom synchrotron measurement, second row neutron data) of SrP_2N_4. The standard deviations are given in parentheses.

Atom	Wyckoff pos.	x	y	z	$U_{iso}\cdot100$
Sr(1)	2a	0	0	0.8493(10)	1.461(18)
		0	0	0.8491(61)	0.52(40)
Sr(2)	6c	0.15256(32)	0.81751(33)	−0.1774(11)	1.461(18)
		0.1517(8)	0.8137(6)	−0.1897(16)	0.93(18)
Sr(3)	6c	0.33433(48)	0.19507(31)	−0.1793(11)	1.461(18)
		0.3304(8)	0.1925(5)	−0.1852(17)	1.82(21)
Sr(4)	2b	1/3	2/3	0.7994(13)	1.461(18)
		1/3	2/3	0.7922(13)	0.49(35)
Sr(5)	2b	1/3	2/3	0.2986(13)	1.461(18)
		1/3	2/3	0.2891(15)	2.89(51)
Sr(6)	6c	0.47842(38)	−0.00435(29)	0.3301(7)	1.461(18)
		0.4844(5)	−0.0083(7)	0.3250(12)	0.62(19)
P(1)	6c	0.1574(10)	0.1683(9)	0.1330(18)	0.378(34)
		0.1582(11)	0.1638(11)	0.1262(16)	1.90(40)
P(2)	6c	0.1671(10)	0.0050(11)	0.0166(17)	0.378(34)
		0.1676(10)	0.0035(10)	0.0118(16)	1.40(39)
P(3)	6c	0.3385(11)	−0.0002(13)	0.0138(13)	0.378(34)
		0.3328(14)	−0.0049(11)	0.0069(13)	2.26(33)
P(4)	6c	0.3356(9)	1.0003(13)	0.6257(14)	0.378(34)
		0.3297(12)	1.0008(13)	0.6227(14)	2.18(33)
P(5)	6c	0.3382(10)	0.8353(9)	0.6354(20)	0.378(34)
		0.3392(11)	0.8294(11)	0.6106(15)	1.24(37)
P(6)	6c	0.3420(9)	0.8319(9)	0.0189(18)	0.378(34)
		0.3341(12)	0.8250(11)	0.0260(17)	1.73(37)
P(7)	6c	0.4944(9)	0.1732(9)	0.6320(18)	0.378(34)
		0.4948(12)	0.1678(11)	0.6463(16)	1.49(40)
P(8)	6c	0.5029(10)	0.1731(10)	0.0055(16)	0.378(34)
		0.5021(12)	0.1746(11)	−0.0054(16)	1.40(38)
N(1)	6c	0.3927(17)	0.7985(22)	0.5330(38)	0.25(9)
		0.4005(8)	0.8041(6)	0.5139(9)	1.59(17)
N(2)	6c	0.0922(19)	0.8966(15)	0.0126(36)	0.25(9)
		0.0925(6)	0.8966(6)	0.0146(9)	1.17(14)
N(3)	6c	0.1268(19)	0.0624(16)	0.1116(37)	0.25(9)
		0.1239(6)	0.0599(7)	0.1134(10)	1.61(16)
N(4)	6c	0.2303(16)	0.9593(15)	0.5793(39)	0.25(9)
		0.2280(7)	0.9613(5)	0.5681(10)	0.87(17)
N(5)	6c	0.2679(18)	0.0302(27)	0.0846(37)	0.25(9)
		0.2659(7)	0.0310(5)	0.0918(9)	0.03(13)
N(6)	6c	0.2592(15)	0.7316(15)	0.0301(34)	0.25(9)
		0.2736(5)	0.7319(6)	0.0321(9)	1.57(17)
N(7)	6c	0.1705(21)	0.0343(22)	−0.1808(25)	0.25(9)
		0.1802(5)	0.0397(5)	−0.1815(12)	1.30(15)
N(8)	6c	0.3092(22)	0.8991(18)	0.0820(40)	0.25(9)
		0.3071(5)	0.9020(8)	0.0770(9)	1.38(18)
N(9)	6c	0.4388(18)	0.0730(17)	0.0829(43)	0.25(9)
		0.4401(5)	0.0656(6)	0.0751(9)	1.52(19)
N(10)	6c	0.3626(24)	0.9325(18)	0.5534(46)	0.25(9)
		0.3632(5)	0.9337(6)	0.5415(9)	0.60(15)
N(11)	6c	0.3766(18)	0.8531(18)	−0.1793(25)	0.25(9)
		0.3788(5)	0.8502(5)	−0.1903(12)	1.33(15)
N(12)	6c	0.4012(18)	0.0996(17)	0.5519(45)	0.25(9)
		0.3980(5)	0.0991(5)	0.5470(8)	0.04(13)
N(13)	6c	0.4191(18)	0.5489(13)	0.1124(38)	0.25(9)
		0.4372(6)	0.5673(5)	0.1111(9)	1.41(15)
N(14)	6c	0.4844(20)	0.1908(18)	−0.1785(24)	0.25(9)
		0.4836(6)	0.1942(5)	−0.1848(13)	1.51(16)
N(15)	6c	0.3257(17)	1.0022(15)	−0.1834(23)	0.25(9)
		0.3323(8)	1.0108(5)	−0.1787(18)	1.82(14)
N(16)	6c	0.4742(19)	0.2317(20)	0.1280(36)	0.25(9)
		0.4824(5)	0.2351(7)	0.1330(10)	1.39(16)

such as SrP_2N_4 it is very difficult to measure individual ^{31}P–^{31}P distances via the direct dipolar coupling because the spin-pair approximation can definitely not be applied. A selective dipolar recoupling of a distinct ^{31}P–^{31}P coupling as recently proposed in reference [67] is circumvented by the small chemical shift differences. In dense spin systems, however, the exchange rate R_{AB} of an through-space zero-quantum exchange experiment is connected with the sum of all distances between ^{31}P(site A) and ^{31}P(site B) as given in Equation (3).[41]

$$R_{AB} = S \cdot \sum_{i \in B} \sum_{j \in A} r_{ij}^{-6} \qquad (3)$$

Here S is composed of constants such as the gyromagnetic ratio, the normalized zero-quantum intensity at $\nu = 0$, and a scaling factor specific for the employed exchange sequence.[41] For the here presented analysis S was used as an overall scaling factor since relative rates already bear the required information. The time-evolution of the zero-quantum intensities can then be described by a master equation. This phenomenological ansatz is called the "rate matrix approach". Thus after the signal assignment the direct dipolar coupling can provide further information about the three-dimensional topology as the spatial arrangement of atoms can be evaluated by comparison of the experimental build-up curves from through-space NMR measurements with theoretical curves calculated from the structure proposal by using Equation (3).

The first step thus is the signal assignment. The $8! = 40320$ possible permutations are already reduced to 3360 as sites corresponding to the signals C and D cannot be distinguished. Despite this reduction the overlap rather complicates the analysis as connectivities can only be assigned to signal groups C and D and not to the individual resonances.

Figure 8 (left) shows a contour plot of a 2D R-TOBSY[42] spectrum of SrP_2N_4 ($\nu_0 = 121.49$ MHz) with a mixing time of 21 ms. For this mixing time off-diagonal peaks arise only for signals of those nuclei that are connected via ^2J coupling due to a nitrogen bridge. The following pairs can immediately be identified from the spectrum: $^{31}P(A)$–$^{31}P(C)$, $^{31}P(A)$–$^{31}P(D)$, $^{31}P(B)$–$^{31}P(C)$, $^{31}P(B)$–$^{31}P(D)$, $^{31}P(B)$–$^{31}P(E)$, $^{31}P(C)$–$^{31}P(D)$, $^{31}P(C)$–$^{31}P(E)$,$^{31}P(D)$–$^{31}P(E)$, while pairs $^{31}P(A)$–$^{31}P(B)$ and $^{31}P(A)$–$^{31}P(E)$ are not present. This information already restricts the 3360 permutations to 64 possible combinations. Correlations between nuclei which by chance have the same shift (namely the three resonances of signal C and two resonances of signal D) cannot be observed in the R-TOBSY spectrum. Therefore, we performed several 2D double-quantum refocused INADEQUATE experiments[43] with varying mixing times. Figure 8 (right) shows exemplarily the INADEQUATE spectrum ($\nu_0 = 202.5$ MHz) with a mixing time of 4 ms. Here ^2J correlated nuclei create a common pair of signals at their sum frequency in the double-quantum dimension. Besides the already known pairs a $^{31}P(C)$–$^{31}P(C')$ correlation can clearly be recognized. A potential $^{31}P(D)$–$^{31}P(D')$ signal pair is difficult to detect as it would arise at the same double quantum frequency as $^{31}P(C)$–$^{31}P(E)$ does. The $^{31}P(A)$–$^{31}P(D)$ coupling which can clearly but weakly be identified in the R-TOBSY spectrum is not visible in the INADEQUATE spectrum due to the smaller signal-to-noise ratio of the latter.

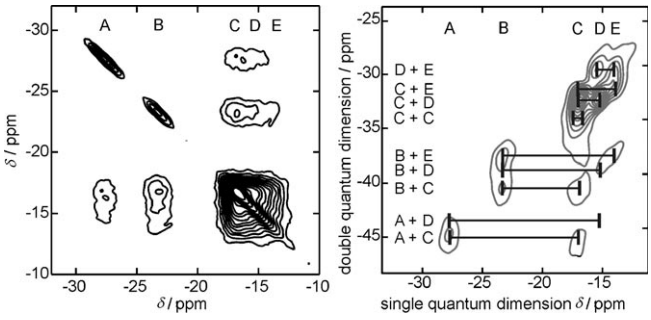

Figure 8. 2D R-TOBSY (left, $\tau_{mix} = 21$ ms, $\nu_0 = 121.5$ MHz) and 2D refocused INADEQUATE experiment (right, $\tau_{mix} = 4$ ms, $\nu_0 = 202.5$ MHz) of SrP_2N_4. Only ^{31}P pairs connected via a nitrogen bridge create in the R-TOBSY spectrum an off-diagonal peak and in the INADEQUATE spectrum a common pair of signals in the double quantum dimension at their sum frequency. These connectivities are indicated by lines. Pair (A + D) is very weak (see R-TOBSY experiment) and thus hardly visible in the INADEQUATE experiment due to a poorer signal-to-noise ratio.

We additionally analyzed the relative intensities of the signals in the INADEQUATE spectra. Under specific conditions they can approximately be correlated with the number of enclosed couplings: 1) anisotropies must be small, which is given for SrP_2N_4 due to the tetrahedral coordination of all ^{31}P atoms; 2) dephasing properties must be similar which can be assumed as all ^{31}P atoms are in a similar chemical environment; 3) the weak coupling limit (chemical shift difference $\gg J$ coupling) must be fulfilled. Strictly speaking, this can not be guaranteed for couplings of the sites in one signal group. However, the chemical shift difference of two sites within one crystallite can be significantly larger than the difference of the isotropic shifts due to the chemical shift anisotropy. The contribution of the concerned signal pairs to an INADEQUATE spectrum can be probed by comparison of the relative signal intensities of the single-quantum projection of the 2D INADEQUATE spectrum with a one-pulse experiment (equal recycle delays) which in our case show a similar signal distribution. Therefore, even the couplings between the three resonances of signal C are not severely reduced despite their tiny isotropic chemical shift differences. Accordingly, we can conclude that the double-quantum intensity of the $^{31}P(C)$–$^{31}P(C')$ pair is lower than of $^{31}P(C)$–$^{31}P(D)$ and thus that more $^{31}P(C)$–$^{31}P(D)$ than $^{31}P(C)$–$^{31}P(C')$ couplings are present. The application of this constraint reduces the number of permutations to 16, which are given in Table 3. These 16 permutations contain exactly the same connectivities between signals A to E which are depicted in Figure 9.

A further restriction within the given signal resolution is thus not possible from J coupling experiments.

For the comparison of the build-up curves calculated from the structure model with through-space exchange experiments a series of 12 2D RIL experiments[30] ($\nu_0 =$

Table 3. The remaining 16 possibilities for assigning the eight crystallographical sites 1 to 8 to NMR signals A to E after selection according to *J* coupling experiments.[a]

Signal					Dev	Signal					Dev
A	B	C	D	E	[%]	A	B	C	D	E	[%]
1	8	2|5|6	4|7	3	0.0	2	6	1|7|8	3|4	5	4.5
2	5	1|7|8	3|6	4	1.0	1	6	2|7|8	3|4	5	4.5
1	6	2|7|8	4|5	3	1.2	2	7	1|5|6	3|4	8	5.0
2	7	1|5|6	3|8	4	1.7	1	7	2|5|6	3|4	8	5.0
2	8	1|5|6	3|4	7	2.9	1	3	2|7|8	4|5	6	7.3
1	8	2|5|6	3|4	7	2.9	1	3	2|5|6	4|7	8	7.4
2	5	1|7|8	3|4	6	3.9	2	4	1|5|6	3|8	7	8.2
1	5	2|7|8	3|4	6	4.1	2	4	1|7|8	3|6	5	9.0

[a] The permutations are sorted according to their fit quality for RIL build-up curves (see Figure 10). The deviation (dev) is calculated by (rms(actual)−rms(best))/(rms(worst)−rms(best)), where rms is the root-mean-square error between calculated and experimental build-up curves.

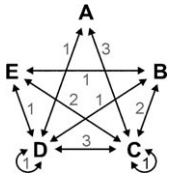

Figure 9. Connectivities between signals A to E in the possible signal assignments remaining after analysis of R-TOBSY and INADEQUATE spectra. The numbers in gray denote the number of couplings between the particular signals. The coupling depicted as circles around C and D stand for correlations between different resonances under the same signal.

202.5 MHz) with mixing times τ_{mix} between 0 and 31 ms was measured. Signal intensities were derived from 2D deconvolutions of all spectra describing the 25 signals via 2D Gauss functions and are depicted as circles in Figure 10. RIL is, in a good approximation, a zero-quantum exchange experiment based on the direct dipolar coupling.[30] As discussed in the literature[41,44] the time-evolution of the peak intensities I_{kl} (build-up curves) can then be calculated within the rate matrix approach, where intensities I_{kl} are given by Equation (4).

$$I_{kl}(\tau_{mix}) = P_{kl}(\tau_{mix})I_{l0} = [\exp(K\tau_{mix})]_{kl}I_{10} \quad (4)$$

Here I_{l0} is the magnetization of spin l before exchange, and K is the kinetic matrix. In our case I_{l0} is not equal to 1 for all signals as we could not fully relax the system due to relaxation times of several thousands of seconds. K_{kl} describes the magnetization transfer from signal l to signal k, while the diagonal element K_{kk} is obtained from Equation (5).

$$K_{kk} = -\sum_{k \neq l} K_{kl} \quad (5)$$

For the simulation of the build-up curves from diffraction data the R_{kl} values were obtained from Equation (3). All distances between ^{31}P(site k) and ^{31}P(site l) within a sphere with radius $r = 60$ Å were included from the diffraction data structure solution. K_{kl} values were then derived from R_{kl} values after weighting with $1/I_{l0}$ to account for unequal intensities. For the calculation of the intensities $I_{kl}(\tau_{mix})$ the now asymmetric kinetic matrix K was symmetrized and diagonalized according to literature.[45] Afterwards build-up curves for all eight crystallographic sites were assigned to the five NMR signals for all 3360 permutations, where sites belonging to the same NMR signal were summed up. The curves were finally fitted to the experimental data with the refinement parameters I_{l0} and S (see Equation (3)). For the fitting procedure only off-diagonal build-up curves were included preventing the high diagonal intensities from dominating the fit. As expected the parameters I_{l0} reproduced the relative intensities of the diagonal peaks in the RIL

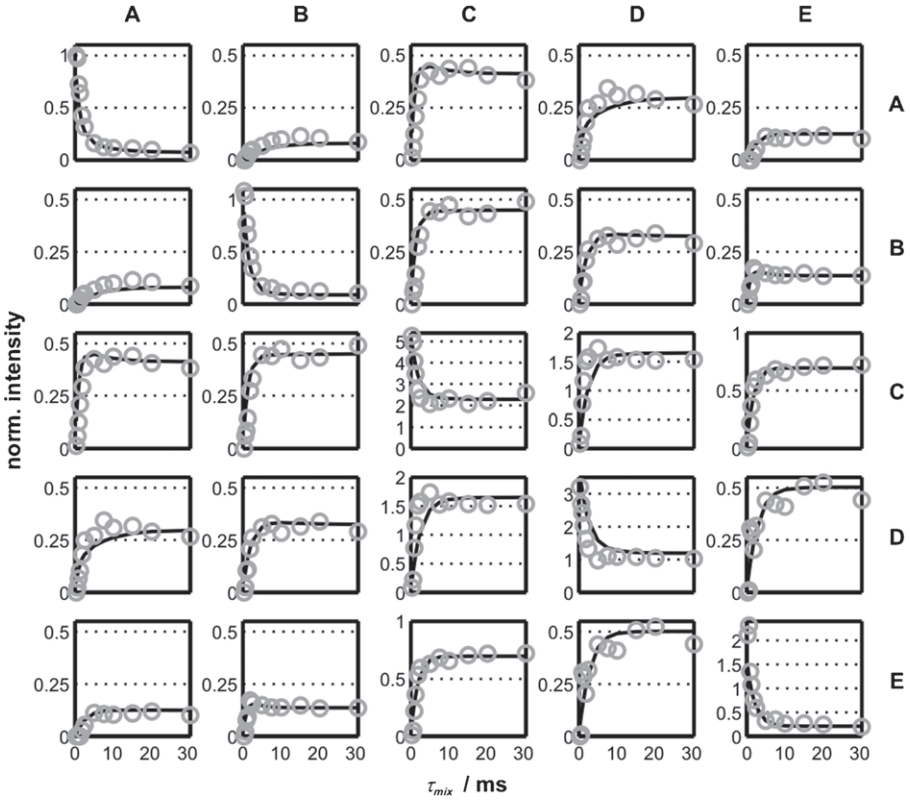

Figure 10. Experimental build-up curves (circles) from RIL experiments and calculated build-up curves (lines) from diffraction data analysis for the best fitting permutation. Build-up curves are arranged like signals in the 2D RIL spectrum (Figure 2c) from top left = A–A to bottom right = E–E.

spectrum with $\tau_{mix} = 0$ ms.

In Figure 10 the build-up curves for the permutation fitting best to the experimental data is shown. This permutation is one of the 16 remaining possibilities from *J* coupling experiments and it represents well the experimental build-up curves. Moreover, all 16 permutations show good agreement with the experimental build-up curves and are situated within the best 9% of all permutations (see Table 3). As the build-up curves reflect the spatial arrangement of the ^{31}P atoms, the NMR data confirms the proposed topology of a three-dimensional network of corner-sharing PN_4 tetrahedrons for all 16 possible assignments. Therefore, the NMR analysis fully supports the diffraction structure solution.

Finally, the difficulties arising from the heavy overlap of the ^{31}P resonances shall be discussed briefly. We have pointed out before that for a fully resolved spectrum an unambiguous assignment of signals would have been possible from *J* coupling experiments. The effects on the analysis of the direct dipolar coupling experiments becomes clear if we consider that within a maximum of the 9% of deviation above the best-fitting permutation (which contains the 16 remaining assignments) there are 55 further permutations. Nearly all of them differ from the 16 remaining possibilities in their number and the existence of couplings of signals C and D. As the build-up curves with signals C and D contain a large number of couplings (due to the contribution of more than one resonance) these are not significantly influenced by these changes and thus still reproduce the experimental data well. If, however, the number of couplings between the resolved resonances differ (^{31}P(A)–^{31}P(B), ^{31}P(A)–^{31}P(E), ^{31}P(B)–^{31}P(E)) the build-up curves change accordingly. This is exemplarily shown in Figure 11 where the build-up curve of the best fitting permutation is compared with permutation no. 322 (for details see caption for Figure 11). The sensitivity of the time-evolution of the zero-quantum transfer is thus substantially reduced by the signal overlap. In conclusion, for the extraction of structural data exceeding topological information, an analysis of the build-up curves must be focussed on well-resolved resonances.

Description of the structure: The framework structure of SrP_2N_4 is isotypic with the TX_2-framework structures (T= tetrahedral coordinated atom, Ga, Al, Si, Ge, Zn, P, Co; X = O) of $BaGa_2O_4$,[17] $KAlGeO_4$,[19] $KCoPO_4$,[46] and $KZnPO_4$,[47] which correspond with the *megakalsilite* ($KAlSiO_4$) structure type[48] being a stuffed framework structure consisting of sequences of tetrahedral layers. Each layer perpendicular to [001] is built up from rings made of six corner-sharing PN_4 tetrahedrons (6-rings). Figure 12 (top) shows an orthographic projection parallel to [001] of one layer (the cations are omitted for clarity). The vertices of the tetrahedrons within a ring (i.e. within a layer) are not strictly coplanar as they are corrugated vertically to the [001] direction. Furthermore, adjacent vertices of the tetrahedrons pointing up or down deviate in pairs parallel to [100] and [010] (emphasized by line "D", Figure 12) and are corrugated vertically to [001] as well. The vertices of these PN_4 tetrahedrons are connected to adjacent layers building up a $PN_{4/2}$ network. Along [001] the tetrahedrons connecting the layers form an energetically favorable staggered conformation. The entire network is made up of two types of

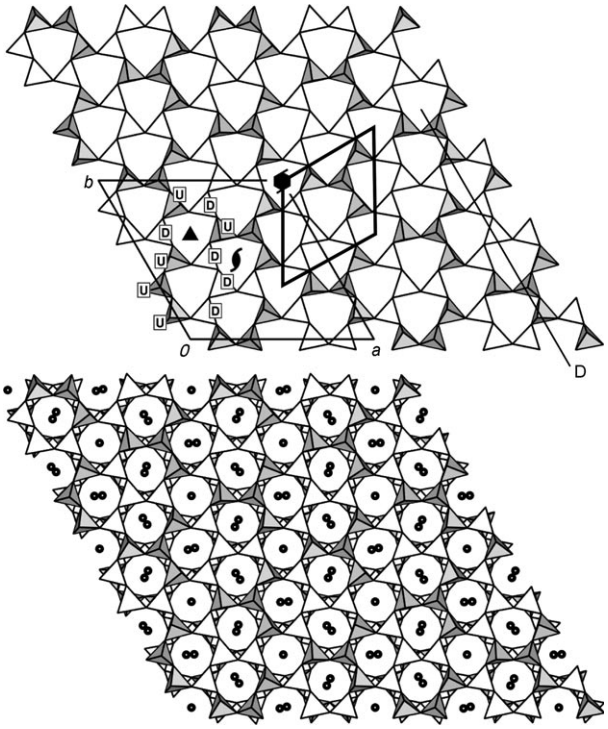

Figure 12. Tetrahedral layer of SrP_2N_4 (perpendicular to [001]) built up of six-membered rings. The up-oriented tetrahedral corners are marked with "U" and the down-oriented with "D". In the upper figure the Sr atoms are left out for clarity; 3/4 of the rings have UUUDDD orientation and 1/4 have UDUDUD orientation. The rings with alternating tetrahedral corners (UDUDUD) are arranged around the 6_3 and 3 axis. The upper figure shows a single layer, the lower figure shows two connected layers AB with Sr^{2+} ions in the cavities. D indicates the deviation line, the bold printed elementary mash is from the basic structure cell, the thin printed from the superstructure cell.

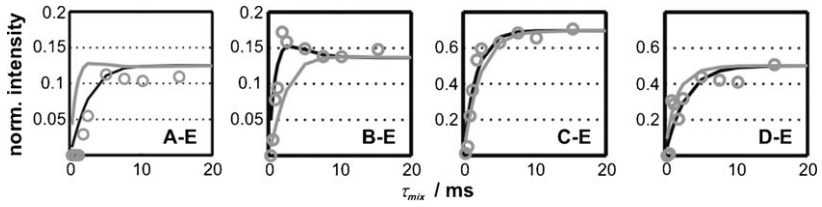

Figure 11. Comparison of the best fitting permutation (A = 1, B = 8, C = 2/5/6, D = 4/7, E = 3) with permutation no. 322 (A = 1, B = 8, C = 2/5/6, D = 3/7, E = 4; dev 27.6%) where the depicted couplings with E all differ in their number by 1. Obviously this has a strong impact on the build-up curves composed of only resolved signals (A and B), while the curves of C and D are only changed slightly.

layers (A and B), which are symmetrically eqivalent.[4] The layers exhibit the *two-dimensional space group* symmetry $P(3)11$.[49] Within a single layer two types of six-membered rings have to be distinguished with respect to the relative orientation of up (U) and down (D) pointing vertices of adjacent tetrahedrons: one fourth of the rings have an UDUDUD topology (Figure 12) and are located about the 6_3 and the 3 axis running parallel to [001]. The remaining rings have an UUUDDD conformation. 1/3 of them (i.e. 1/4 of *all* rings) surround the 2_1 axis (Figure 12). Furthermore, there are 4-rings, 8-rings and 10-rings perpendicular to [210] and [120]. The cycle-class sequence (i.e. the relative frequency of the P_nN_n ring sizes occurring in the network for $n=1, 2, 3, \ldots$) has been calculated with the program TOPOLAN[50] and it amounts to {–, 0, 0, 6, 0, 16, 0, 42, 0, 96, …}. The framework density[31] of SrP_2N_4 has a value of 23.38 T/1000 Å^3 and corresponds to those of other highly condensed nitridophosphates, for example, $BaSr_2P_6N_{12}$[3] with 23.5, $BaCa_2P_3N_6$ with 24.31,[3] or BaP_2N_4[2] with 22.42 T/1000 Å^3. It is noteworthy that the crystal structure shows distinct pseudosymmetry as it is almost describable in space group $P6_322$. The two-dimensional space group symmetry of the layers would then be $P(3)21$,[49] originating from twofold axes about [120] and [100]. In that case the connection of the layers would be established over energetically unfavorable 180° P-N-P bridges (1/3 of all interlayer P-N-P bridges, basic cell). Furthermore, the existence of pseudo-twofold axes explains why the crystals are subject to twinning. Considering only the P–N framework, one more step to higher symmetry is space group $P6_3/mcm$, which does not allow the corrugation of the layers. The highest possible topological symmetry of the structure type (aristotype) is established in the subcell with space group $P6_3/mmc$,[17] which turns the staggered conformation of the tetrahedrons to an eclipsed one. The size of the subcell and the supercell are described by the following axis transformation: $a'=2a+b$; $b'=-a+b$; $c'=c$. Based on the synchrotron diffraction data the P–N bond distances in SrP_2N_4 vary between 1.46(3) and 1.81(3) Å. The neutron powder diffraction data refinement shows P–N distances in the range 1.45(2) to 1.87(2) Å. We note that a remarkable wide range of P–N bond lengths occurs in SrP_2N_4. Usually these values range between 1.55–1.70 Å (e.g. HPN_2: 1.599(4) Å,[5] $LiPN_2$: 1.645(7) Å,[7] BaP_2N_4: 1.630(6)-1.661(7) Å[2]). However, a distance-least-squares (DLS) refinement[51] led to a smaller distribution of the P–N bond length and the resulting structural model exhibits a significantly worse agreement with the measured diffraction data.

In the structure there are two types of voids filled with Sr^{2+} ions. The first type is formed by two UDUDUD six-rings along the 6_3 screw or 3 rotation axes (Figure 13). The voids provide almost spherical coordination for Sr(1), Sr(4), and Sr(5) with a $3+3+3=9$ coordination sphere (see Figure 13, for example Sr(4)). These voids are quite similar in their dimensions. The inner diameter of the void built by

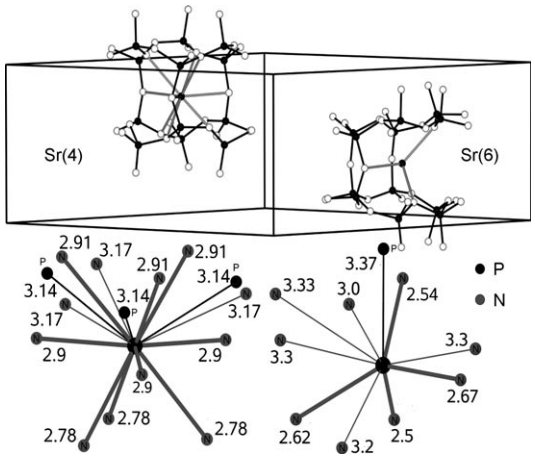

Figure 13. Two exemplary voids in the framework of of SrP_2N_4 (view almost perpendicular to [110]) as well as coordination of Sr(4) and Sr(6). The upper left void is formed by two UDUDUD rings (Sr(4)), the lower right void is formed by two UUUDDD rings (Sr(6)). The tetrahedrally coordinated P atoms are drawn in black, the N atoms in gray, and the Sr atoms in the center of the void are drawn in black as well. The Sr–N distances belonging to the coordination sphere are drawn with thick lines, the longer distances lying out of the coordination sphere are marked with thin lines. The Sr–N distances are taken from synchrotron diffraction data.

three N(7) atoms surrounding Sr(1) almost equatorially (Figure 13) is 2.67 Å and the three N(3) atoms building an equilateral triangle and closing the voids at the top and the bottom, respectively, permit a diameter[5] of only 1.88 Å. The void belonging to Sr(4) is built up of N(11) providing a diameter of 2.89 Å and closed by triangles of N(6) (diameter of 2.06 Å) and N(1) (diameter of 1.96 Å). Sr(5) is coordinated with the same atoms (N(1), N(6), N(11), and N(14)) in a similar manner. The Sr–N distances of the voids built up of UDUDUD rings vary around 2.683(31) Å (Sr(1)–N(7)) and 2.997(24) Å (Sr(5)–N(6)).

The second type of void encloses Sr(2), Sr(3), and Sr(6). These voids are built up of two UUUDDD six-membered rings. In contrast to the first type, these voids are "open" at one side and to not provide a closed coordination shell (Figure 13, example Sr(6)). Only four short ($<$ 2.7 Å) Sr(6)–N distances occur, which form a distorted tetrahedron and are much shorter than the respective Sr–N distances of Sr(1), Sr(4), and Sr(5). Together with two long distances, Sr(6) has a $4+2$ coordination. Interestingly the $5+1$ coordination of Sr(2) (distorted octahedron) is quite similar to the coordination of Sr atoms in SrN[52] with five short distances varying around 2.56–2.88 Å and one long distance of 3.13 Å. The coordination of Sr(3) is similar to that of Sr(6). Only at first glance the coordination of Sr(2, 3, 6) in SrP_2N_4 is unfavorable. Admittedly the ninefold coordination of Sr(1, 4, 5) is almost spherical and provides a "closed" coordination sphere, but the Sr–N distances for Sr(1), Sr(4), and Sr(5)

[4] The layers can be transferred into each other by a 60° rotation about [001] and translation of [0 0 $^1/_2$].

[5] We define the "diameter" of a void in this structure as the largest circle that can be inscribed in an equilateral triangle built up of three N atoms.

are much longer than the Sr–N distances for Sr(2), Sr(3), and Sr(6) in the voids formed by UUUDDD rings. A sufficient coordination of Sr(2, 3, 6) is also supported by the results of valence sum[53] calculations. The valence sums[53] for the cations Sr(1, 4, 5) (between UDUDUD rings) amount to 2.56, 1.88, and 1.87, respectively. The valence sums[53] for Sr(2), Sr(3), and Sr(6) (between UUUDDD rings) amount to 1.95, 1.86, and 2.09, respectively. The multiplicity weighted average valence sum of a Sr atom is very close to the ideal value of 2.0 and amounts to 1.99. The valence sum variation of those Sr atoms, which are encapsulated in tridymite-like voids formed by UDUDUD rings is actually greater than the variation of the valence sums of the more "unfavorably" encapsulated atoms in voids built up of UUUDDD rings (calculated with the bond valence parameters provided by O'Keeffe et al.[54] and interatomic distances obtained from the synchrotron measurement, Table 4). These observations lead us to the question, why this structure type is formed and not one of the various stuffed tridymite-type framework structures. We think that the main reason is the value of the P-N-P angles of the N atoms connecting the layers, P(1)-N(7)-P(2), P(3)-N(15)-P(4), P(5)-N(11)-P(6), and P(7)-N(14)-P(8), which vary between 142(2) and 164(2)° (Table 5). The tridymite topology does not provide angles much smaller than 170° between the hexagonal layers (even in *low* tridymite-type frameworks) without distorting the tetrahedral coordination of the P atoms too much, whereas the megakalsilite topology established here, *does* provide such smaller angles, known from all highly condensed nitridophosphates by *corrugating* the layers. However, the P-N-P angles within the layers are much smaller and range between 124.7(21) and 136.9(23) as shown in Table 5 (synchrotron measurement). Increasing the average diameter of the incorporated cations leads to a completely different structure type. Small P-N-P angles can then be achieved by forming three-rings as building units as observed in $BaSr_2P_6N_{12}$,[3] $BaCa_2P_6N_{12}$,[3] and BaP_2N_4.[2] Another example for an AB_2X_4 structure type with corrugated layers and comparatively small T-X-T angles may be $BaFe_2O_4$-II,[55] which has layers of UUDUDD 6-rings and Fe-O-Fe angles between 114(2) and 158(2)°.

Table 4. Sr–N distances (in Å, synchrotron data refinement) in SrP_2N_4 taken for the valence sum calculations, standard deviations in parentheses.

Atoms	Distance	Atoms	Distance
Sr(1)–N(2)	3.187(30)	Sr(4)–N(1)	2.914(34)
Sr(1)–N(3)	2.836(32)	Sr(4)–N(6)	2.781(29)
Sr(1)–N(3)	2.690(28)	Sr(4)–N(6)	2.782(29)
Sr(1)–N(3)	2.836(32)	Sr(4)–N(11)	2.895(26)
Sr(1)–N(3)	2.690(28)	Sr(4)–N(11)	2.896(26)
Sr(1)–N(3)	2.836(32)	Sr(4)–N(11)	2.897(26)
Sr(1)–N(3)	2.690(28)	Sr(4)–N(16)	3.173(28)
Sr(1)–N(7)	2.683(31)	Sr(4)–N(16)	3.171(28)
Sr(2)–N(2)	2.581(27)	Sr(5)–N(1)	2.726(31)
Sr(2)–N(4)	2.883(28)	Sr(5)–N(1)	2.727(31)
Sr(2)–N(5)	2.649(30)	Sr(5)–N(6)	2.996(24)
Sr(2)–N(8)	3.13(4)	Sr(5)–N(6)	2.997(24)
Sr(2)–N(9)	3.34(4)	Sr(5)–N(13)	3.384(21)
Sr(2)–N(12)	2.565(31)	Sr(5)–N(13)	3.382(21)
Sr(2)–N(15)	3.065(25)	Sr(5)–N(14)	2.845(29)
Sr(2)–N(16)	2.600(30)	Sr(5)–N(14)	2.844(29)
Sr(3)–N(2)	3.284(32)	Sr(6)–N(1)	3.359(33)
Sr(3)–N(4)	2.565(31)	Sr(6)–N(8)	3.22(4)
Sr(3)–N(5)	3.26(4)	Sr(6)–N(9)	2.668(29)
Sr(3)–N(5)	3.16(4)	Sr(6)–N(9)	3.04(4)
Sr(3)–N(7)	2.776(32)	Sr(6)–N(10)	2.495(31)
Sr(3)–N(8)	2.589(29)	Sr(6)–N(10)	3.25(4)
Sr(3)–N(10)	3.12(4)	Sr(6)–N(11)	2.536(27)
Sr(3)–N(12)	3.25(4)	Sr(6)–N(12)	3.24(4)
Sr(3)–N(14)	2.604(30)	Sr(6)–N(13)	2.632(32)
Sr(3)–N(15)	3.227(22)	Sr(6)–N(13)	3.030(24)
Sr(4)–N(1)	2.913(34)	Sr(6)–N(15)	3.334(26)

Table 5. P-N-P angles [°] of SrP_2N_4, standard deviations in parentheses. The interlayer angles are printed in bold letters.

Atoms	SrP_2N_4 (sync.)	SrP_2N_4 (neut.)
P(1)-N(2)-P(2)	127.9(18)	130.7(10)
P(1)-N(3)-P(2)	135.8(22)	130.7(9)
P(1)-N(4)-P(4)	123.4(18)	123.7(11)
P(1)-N(7)-P(2)	**149.2(24)**	**142.9(10)**
P(2)-N(5)-P(3)	129.8(20)	121.3(9)
P(3)-N(8)-P(6)	128.3(20)	133.3(10)
P(3)-N(9)-P(8)	124.7(21)	119.8(10)
P(3)-N(15)-P(4)	**164.4(19)**	**164.4(14)**
P(4)-N(10)-P(5)	125.6(22)	127.4(9)
P(4)-N(12)-P(7)	125.2(22)	119.6(9)
P(5)-N(1)-P(8)	136.9(23)	143.5(9)
P(5)-N(11)-P(6)	**141.5(20)**	**139.3(9)**
P(5)-N(16)-P(8)	133.2(21)	124.9(9)
P(6)-N(6)-P(7)	138.0(21)	127.7(13)
P(6)-N(13)-P(7)	131.8(20)	133.1(11)
P(7)-N(14)-P(8)	**145.3(21)**	**136.4(14)**

Whereas $BaGa_2O_4$,[56] KZn_2O_4,[57] and megakalsilite ($KAlSiO_4$)[58] undergo second-order phase transitions forming tridymite related frameworks upon heating, SrP_2N_4 decomposes above 1100 °C at ambient pressure. A DTA investigation gave no evidence of any phase transition below the decomposition temperature, so we can conclude that the polymorph we obtained by high-pressure, high-temperature synthesis is not a quenched high-pressure phase.

It is noteworthy, that we identified a cubic phase with the composition "SrP_2N_4" in the product of the reaction between KN_3, $Sr(N_3)_2$, and P_3N_5 in a molar ratio of 1:1:1 at 5 GPa and 1300 °C together with hexagonal SrP_2N_4 and other, amorphous phases. Electron diffraction experiments showed that the lattice parameter *a* of that cubic phase amounts to about 10 Å. The respective parameter of $BaSr_2P_6N_{12}$ is 10.0705(2) Å,[3] of BaP_2N_4 is 10.22993(2)[2] and of $BaCa_2P_6N_{12}$ is 9.9578(2) Å.[3] Thus, we presume the existence of a cubic SrP_2N_4 phase being isotypic to BaP_2N_4[2] with a cell volume near to 1000 Å^3 and a slightly higher density of 4.097 g cm^{-3}.

Experimental Section

Synthesis of phosphorus(V) nitride: Partially crystalline phosphorus(V) nitride was obtained by the reaction of gaseous ammonia with

hexachlorocyclotriphosphazene $(PNCl_2)_3$ (Merck, p. a.) following the procedure given in the literature.[23] The reaction was carried out at 950 °C in a gas flow of dried ammonia (dried by flowing through a column (l = 1000 mm, $\varnothing$ = 50 mm) filled with KOH pellets).

Synthesis of strontium azide: Strontium azide was obtained by the reaction of strontium carbonate (Merck, p. a.) with an aqueous solution of HN_3, synthesized from NaN_3 (Merck, p. a.) and H_2SO_4 by destillation, in accordance with reference [59]. It was dried over P_4O_{10} using a vacuum desiccator. A general procedure to yield azides of the heavy alkaline-earth elements is described in reference [60].

Synthesis of SrP_2N_4: The high-pressure synthesis of SrP_2N_4 was carried out using the multianvil[24,25,61] technique and a hydraulic press according to Equation (2). Cr_2O_3-doped MgO octahedra (Ceramic Substrates & Components LTD., Isle of Wight) with an edge length of 18 mm were used. Eight truncated tungsten carbide cubes separated by pyrophyllite gaskets served as anvils for the compression of the octahedra. The truncation edge length was 11 mm. A mixture of strontium azide and partially crystalline phosphorus(V) nitride,[23] was ground thoroughly in a ball mill and loaded into a cylindrical capsule of hexagonal boron nitride (Henze, Kempten) with a capacity of 35 mm^3 and sealed with a BN cap. The capsule was centered within two nested graphite tubes, which acted as an electrical resistance furnace. The remaining volume at both ends of the sample capsule was filled out with two cylindrical pieces of magnesium oxide. The arrangement was placed into a zirconium dioxide tube and then transferred into a pierced MgO octahedron. The electrical contact of the graphite tubes was arranged through two plates of molybdenum. The assembly was compressed up to 5 GPa at room temperature within 3 h and then heated up to 1400 °C over 25 min. Under these conditions the sample was treated for 40 min and finally cooled down to room temperature over 70 min. Subsequently, the pressure was released over a period of seven hours. By using this procedure about 75 to 95 mg of SrP_2N_4 was obtained as a colorless and crystalline powder. The temperature was calculated from the electrical power applied to the furnace, which was determined on the basis of calibration curves from measurements with $W_{97}Re_3W_{75}Re_{25}$ thermocouples, as described in reference [62].

Electron diffraction experiments: For electron diffraction patterns (SAD, selected area diffraction) and high-resolution images a transmission electron microscope (Philips, CM30/ST) was used. The acceleration voltage was 300 kV, the spherical aberration constant C_s of the device was 1.15 mm, and the point resolution was 0.19 nm. Samples were finely ground and images were taken from thin regions near crystallite edges. The analysis and interpretation of the diffraction images and the computation of simulations were conducted by using the EMS[36] program package.

NMR experiments: ^{31}P MAS spectra were recorded at ambient temperature on the conventional impulse spectrometers Avance II 750, DSX Avance 500, and Avance II 300 (all Bruker) corresponding to ^{31}P Larmor frequencies of ν_0 = 303.7, 202.5, and 121.5 MHz, respectively. Samples were contained in standard 2.5-mm ZrO_2 rotors, which were mounted in standard double-resonance MAS probes (Bruker). ^{31}P signals are referenced with respect to 85 % H_3PO_4. 1D MAS spectra were recorded with $\pi/2$ pulse durations about 2 μs and recycle times of 6000 to 8000 s to guarantee full T_1-relaxation. A series of 12 2D RIL[30] spectra was performed at ν_0 = 202.5 MHz with mixing times in the range of 0.3 to 30.7 ms. $\pi/2$ pulse durations of 1.8 μs and recycle delays of 300 s were employed. t_1 was incremented rotorsynchronized (80 μs) at a spinning frequency of 12.5 kHz. The R-TOBSY spectrum (ν_0 = 121.5 MHz) was recorded as described in reference [42]. The abbreviation R-TOBSY therein corresponds to the symmetry-based pulse sequence[63] $R30_6^{14}$. The experiment was performed with additional z-filters of 30 ms directly before and after the $R30_6^{14}$ blocks. A spinning frequency of 15 kHz was used resulting in a nutation frequency of 75 kHz for the $R30_6^{14}$ blocks. The mixing time was set to 21 ms and t_1 increments to 133.33 μs at a recycle time of 450 s. The 2D refocused INADEQUATE spectrum was measured according to reference [43] at ν_0 = 202.5 MHz. $\pi/2$ pulse durations were set to 1.7 μs, the delay τ to 4 ms, and the recycle time to 250 s. Coherence pathway selection was performed by using the Cogwheel phase cycle[64] COG12-(5,8,9;3). Twelve transients were recorded per increment with a t_1 increment of 50 μs at a spinning frequency of 20 kHz. Some additional INADEQUATE experiments (not shown) were recorded on a DSX Avance 400 (ν_0 = 161.5 MHz) with standard 4-mm ZrO_2 rotors. Spinning frequencies were around 15 kHz. Here mixing times were varied between 2 and 6 ms.

Powder diffraction experiments: Synchrotron diffraction data (wavelength 0.7996003 Å) were acquired at the *S*wiss *N*orwegian *B*eamline (SNBL), ESRF, Grenoble, France (see Table 1) in Debye-Scherrer geometry (diameter of the glass capillary (Hilgenberg, Malsfeld) 1.0 mm). The model-biased LeBail intensity extraction was performed with the LeBail routine in the program package GSAS[32] using the EXPGUI[65] interface. The subroutine "*reflist*" allowed us to write the model-biased F_o^2 to a file. The F_o^2 were scaled and converted to *hklf4* format suitable for SHELXS[35] using *gsa2hklf*. The difference Fourier maps were calculated by the subroutines "*forplot*", "*forsrh*", and "*fourier*" of the program package GSAS.[32] Neutron diffraction experiments were carried out with the D20 diffractometer at the *I*nstitut *L*aue *L*angevin (ILL) in Grenoble, France, with a constant wavelength of 1.8893(1) Å and a cylindrical sample holder with a diameter of 5 mm made of niobium (Debye-Scherrer geometry). Laboratory diffraction experiments were carried out at a Stoe StadiP (Stoe & Cie., Darmstadt) diffractometer equipped with a copper X-ray tube ($Cu_{K\alpha 1}$ radiation, Ge(111) monochromator) and PSD counter ($\Delta 2\theta$ = 5°) using glass capillaries with a diameter of 0.3 mm (Hilgenberg, Malsfeld).

Acknowledgements

Generous financial support by the "Fonds der Chemischen Industrie" (FCI) and the "Deutsche Forschungsgemeinschaft" (DFG), projects SCHN 377/11–1 and SE 1417/1–1, is gratefully acknowledged. We further would like to thank Dr. Hermann Emrich, SNBL beamline, Grenoble France, for his help solving some instrumental problems on Sunday afternoon, Dr. Thomas Hansen, ILL Grenoble, France for his assistance in acquiring the neutron diffraction data, Professor Arndt Simon, Max-Planck-Institut für Festkörperforschung, Stuttgart, Germany, for giving us the possibility of performing electron diffraction/TEM experiments, and Viola Duppel for her technical support for these experiments. Furthermore, we would like to thank Dr. Stefan Steuernagel, Bruker Karlsruhe, for measuring the NMR spectrum of SrP_2N_4 at 303.7 MHz, and Prof. Schweda, Tübingen, for performing the DTA measurements with SrP_2N_4. Finally we thank Prof. Kay Saalwächter for his valuable discussions concerning the NMR experiments.

[1] N. E. Brese, F. J. DiSalvo, *J. Solid State Chem.* **1995**, *120*, 378–380.
[2] F. Karau, W. Schnick, *J. Solid State Chem.* **2005**, *178*, 135–141.
[3] F. Karau, W. Schnick, *Z. Anorg. Allg. Chem.* **2006**, *632*, 231–237.
[4] F. Karau, W. Schnick, *Angew. Chem.* **2006**, *118*, 4617–4620; *Angew. Chem. Int. Ed.* **2006**, *45*, 4505–4508.
[5] W. Schnick, J. Lücke, *Z. Anorg. Allg. Chem.* **1992**, *610*, 121–126.
[6] N. Jacobs, R. Nymwegen, S. Doyle, T. Wroblewski, W. Kockelmann, *Z. Anorg. Allg. Chem.* **1997**, *623*, 1467–1474.
[7] W. Schnick, J. Lücke, *Z. Anorg. Allg. Chem.* **1990**, *588*, 19–25.
[8] P. Eckerlin, C. Langereis, I. Maak, A. Rabenau, *Angew. Chem.* **1960**, *72*, 268; P. Eckerlin, C. Langereis, I. Maak, A. Rabenau, in *Special Ceramics, Vol. 3* (Ed.: P. Popper) Academic Press, London, **1965**, pp. 79.
[9] A. Vitola, J. Ronis, T. Millers, *Latv. PSR Zinat. Akad. Vestis, Kim. Ser.* **1990**, 35–40.
[10] K. Landskron, S. Schmid, W. Schnick, *Z. Anorg. Allg. Chem.* **2001**, *627*, 2469–2472.
[11] W. Schnick, J. Lücke, *Z. Anorg. Allg. Chem.* **1994**, *620*, 2014–2019.
[12] F. Karau, O. Oeckler, F. Schäfers, R. Niewa, W. Schnick, *Z. Anorg. Allg. Chem.* **2007**, *633*, in press.
[13] W. Schnick, N. Stock, J. Lücke, M. Volkmann, M. Jansen, *Z. Anorg. Allg. Chem.* **1995**, *621*, 987–992.
[14] F. Wester, W. Schnick, *Z. Anorg. Allg. Chem.* **1996**, *622*, 1281–1286.

[15] W. Schnick, J. Lücke, *Angew. Chem.* **1992**, *104*, 208–209; *Angew. Chem. Int. Ed. Engl.* **1992**, *31*, 213–215.
[16] N. Stock, E. Irran, W. Schnick, *Chem. Eur. J.* **1998**, *4*, 1822–1828.
[17] V. Kahlenberg, R. X. Fischer, J. B. Parise, *J. Solid State Chem.* **2000**, *154*, 612–618.
[18] B. Eisenmann, M. Jankowski, H. Schäfer, *Mater. Res. Bull.* **1982**, *17*, 1169–1172.
[19] P. A. Sandomirskii, S. S. Meshalkin, I. V. Rozhdestvenskaya, L. M. Dem′yanets, T. G. Uvarova, *Kristallografiya* **1986**, *31*, 883–891.
[20] M. Marezio, J. P. Remeika, P. D. Dernier, *Acta Crystallogr. Sect. A* **1969**, *B25*, 965–970.
[21] J. Dutour, N. Guillou, C. Huguenard, F. Taulelle, C. Mellot-Draznieks, G. Ferey, *Solid State Sci.* **2004**, *6*, 1059–1067.
[22] T. Loiseau, L. Lecroq, C. Volkringer, J. Marrot, G. Ferey, M. Haouas, F. Taulelle, S. Bourelly, P. L. Llewellyn, M. Latroche, *J. Am. Chem. Soc.* **2006**, *128*, 10223–10230.
[23] V. Schultz-Coulon, W. Schnick, *Z. Anorg. Allg. Chem.* **1997**, *623*, 69–74.
[24] H. Huppertz, *Z. Kristallogr.* **2004**, *219*, 330–338.
[25] D. Walker, M. A. Carpenter, C. M. Hitch, *Am. Mineral.* **1990**, *75*, 1020–1028.
[26] K. Landskron, *Dissertation*, Ludwig-Maximilians-Universität, München, **2001**.
[27] P.-E. Werner, *Z. Kristallogr.* **1964**, *120*, 375–387.
[28] J. W. Visser, *J. Appl. Crystallogr.* **1969**, *2*, 89–95.
[29] F. Taulelle, *Solid State Sci.* **2004**, *6*, 1053–1057.
[30] M. Baldus, B. H. Meier, *J. Magn. Reson.* **1997**, *128*, 172–193.
[31] G. O. Brunner, W. M. Meier, *Nature* **1989**, *337*, 146–147.
[32] A. C. Larson, R. B. v. Dreele, *Los Alamos Sci. Lab. [Rep.] LA* **2000**, 86–748.
[33] A. LeBail, *J. Solid State Chem.* **1989**, *83*, 267–271.
[34] A. LeBail, J.-P. Laval, *Can. J. Earth Sci. Eu. J. Solid State Inorg. Chem.* **1998**, *35*, 357–372.
[35] G. M. Sheldrick, University of Göttingen, *Germany.*
[36] P. Stadelmann, *Ultramicroscopy* **1987**, *21*, 131–145.
[37] D. H. Brouwer, R. J. Darton, R. E. Morris, M. H. Levitt, *J. Am. Chem. Soc.* **2005**, *127*, 10365–10370.
[38] W. A. Dollase, M. Feike, H. Förster, T. Schaller, I. Schnell, A. Sebald, S. Steuernagel, *J. Am. Chem. Soc.* **1997**, *119*, 3807–3810.
[39] S. Dusold, J. Kümmerlen, T. Schaller, A. Sebald, W. A. Dollase, *J. Phys. Chem.* **1997**, *B101*, 6359–6366.
[40] X. Helluy, C. Marichal, A. Sebald, *J. Phys. Chem.* **2000**, *B104*, 2836–2845.
[41] P. Robyr, M. Tomaselli, J. Straka, C. Grob-Pisano, U. W. Suter, B. H. Meier, R. R. Ernst, *Mol. Physics* **1995**, *84*, 995–1020.
[42] J. C. C. Chan, G. Brunklaus, *Chem. Phys. Lett.* **2001**, *349*, 104–112.
[43] A. Lesage, M. Bardet, L. Emsley, *J. Am. Chem. Soc.* **1999**, *121*, 10987–10993.
[44] B. Elena, L. Emsley, *J. Am. Chem. Soc.* **2005**, *127*, 9140–9146.
[45] J. Senker, *Solid State Nucl. Magn. Reson.* **2004**, *26*, 22–35.
[46] M. Lujan, F. Kubel, H. Schmid, *Z. Naturforsch. B* **1994**, *49*, 1256–1262.
[47] M. Andratschke, K. J. Range, H. Haase, U. Klement, *Z. Naturforsch. B* **1992**, *47*, 1249–1254.
[48] A. P. Khomyakov, G. N. Nechelyustov, E. Sokolova, E. Bonaccorsi, S. Merlino, M. Pasero, *Canadian Mineral.* **2002**, *40*, 961–970.
[49] H. Grell, C. Krause, J. Grell, *Tables of the 80 plane space groups in three dimensions*, Institut für Informatik und Rechentechnik der Akademie der Wissenschaften der DDR, **1988**.
[50] G. Thimm, S. Schumacher, W. Uhr, W. E. Klee, TOPOLAN, Topological analysis of crystal structures, Institut für Kristallographie der Universität Karlsruhe, Germany **2001**.
[51] C. Baerlocher, A. Hepp, W. M. Meier, DLS-76, a program for the simulation of crystal structures by geometric refinement **1977**.
[52] G. Auffermann, Y. Prots, R. Kniep, *Angew. Chem.* **2001**, *113*, 565–567; *Angew. Chem. Int. Ed.* **2001**, *40*, 547–549.
[53] I. D. Brown, D. Altermatt, *Acta Crystallogr. Sect. B* **1985**, *41*, 244–247.
[54] N. E. Brese, M. O'Keeffe, *Acta Crystallogr. Sect. B* **1990**, *47*, 192–197.
[55] W. Leib, H. Müller-Buschbaum, *Z. Anorg. Allg. Chem.* **1986**, *538*, 71–78.
[56] V. Kahlenberg, C. Weidenthaler, *Solid State Sci.* **2002**, *4*, 963–968.
[57] G. Wallez, F. Lucas, J. P. Souron, M. Quarton, *Mater. Res. Bull.* **1999**, *34*, 1251–1261.
[58] A. J. Perrotta, S. M. Smith, J. V. Smith, *Mineral. Mag. J. Mineral. Soc. (1876-1968)* **1965**, *35*, 588–617.
[59] R. Steudel, P. W. Schenk, in *Handbuch der Präparativen Anorganischen Chemie, Vol. 1*, 3rd ed. (Ed.: G. Brauer), Ferdinand Enke Verlag, Stuttgart, **1978**, p. 456.
[60] P. Ehrlich, H. J. Seifert, in *Handbuch der Präparativen Anorganischen Chemie, Vol. 2*, 3rd ed. (Ed.: G. Brauer), Ferdinand Enke Verlag, Stuttgart, **1978**, p. 930.
[61] D. Walker, *Am. Mineral.* **1991**, *76*, 1092–1100.
[62] D. C. Rubie, *Phase Transitions* **1999**, *68*, 431–451.
[63] M. Carravetta, M. Edén, X. Zhao, A. Brinkmann, M. H. Levitt, *Chem. Phys. Lett.* **2000**, *321*, 205–215.
[64] M. H. Levitt, P. K. Madhu, C. E. Hughes, *J. Magn. Reson.* **2002**, *155*, 300–306.
[65] B. H. Toby, *J. Appl. Crystallogr.* **2001**, *34*, 210–213.
[66] N. N. Lobanov, L. A. d. Veiga, in *6th EPDIC, Abstract, Aug.22–25*, **1998**, pp. 12–16.
[67] I. Marin-Montesinos, G. Mollica, M. Carravetta, A. Gansmüller, G. Pileio, M. Bechmann, A. Sebald, M. H. Levitt, *Chem. Phys. Lett.* **2006**, *432*, 572–578.

Received: February 6, 2007
Published online: June 13, 2007

